# Improving the Performance of Spot Welds in Galvanized Steel Sheets using RGO Reinforcement and Recycled CK45 Steel Chips: A Step Toward Green Welding

Sayyed Mohammadreza Sedehi[*1] ⓘ, Mohammadreza Maraki[2], Masoud Jafarpour[3], Ali Jalali[4], Iman Taheridoustabad[4], Alisina Mortezaei Moghadam[5]

[1] School of Mechanical Engineering, College of Engineering, University of Tehran, Tehran, Iran.
[2] Department of Materials Engineering, Birjand University of Technology, Birjand, Iran.
[3] Master of Science in Materials Engineering, Welding Major, Faculty of Materials Engineering, Sirjan Azad University, Sirjan, Iran.
[4] Department of Mechanical Engineering, Birjand University of Technology, Birjand, Iran.
[5] Department of Mechanical Engineering, Isfahan University of Technology, Isfahan, Iran.

**ARTICLE INFO**

**Article Type**
Original Research

**ABSTRACT**

In this study, in order to enhance the properties of spot-welded galvanized steel sheets and promote the optimal use of industrial waste, machining chips of CK45 steel with thicknesses of 0.2, 0.3, and 0.4 mm were recycled. After selecting the most suitable chip size, the recycled chips were combined with 0.5 wt% reduced graphene oxide (RGO) using a ball milling device and converted into a uniform powder. This composite powder, along with 1 wt% natural tragacanth gum as a binder, was locally applied to the spot welding zone to investigate its effects on the mechanical and corrosion properties of the welds. The test results showed that the reinforced samples exhibited up to a 25% increase in tensile strength (from 3200 N to 4000 N) and up to a 70% reduction in corrosion rate compared to the unreinforced reference samples. This significant improvement is attributed to a more uniform structure, reduced local defects, and improved heat distribution in the weld area. Furthermore, utilizing CK45 steel machining waste as a raw material represents an effective step toward industrial waste management and cost reduction. This novel and environmentally friendly approach has the potential to enhance the durability and quality of spot welds in automotive, construction, and coated sheet metal industries.

**How to cite this article**
Sedehi S.M.R, Maraki M, jafarpour M, Jalali A, Taheridoustabad I, Mortezaei Moghadam A.S, Improving the Performance of Spot Welds in Galvanized Steel Sheets Using RGO Reinforcement and Recycled CK45 Steel Chips: A Step Toward Green Welding. Modares Mechanical Engineering; *2025;25(11):725-734.*

*Corresponding author's email: mrsedehi@ut.ac.ir*
*Corresponding ORCID ID: 0009-0006-5714-7451*

## 1- Introduction

In recent years, the enhancement of the mechanical and metallurgical properties of spot-welded joints, particularly in the automotive and construction industries, has emerged as a major research challenge [1,2]. Due to its high speed, low cost, and automation capability, spot welding is one of the most widely used methods for joining metal sheets, especially galvanized steels [3]. Galvanized steel, which features a protective zinc (Zn) coating, is extensively employed across various industries including automotive [4], construction [5], household appliances [6], and energy sectors [7]. The zinc coating, applied via hot-dip or electro-galvanizing processes, plays a crucial role in protecting the substrate from environmental corrosion, moisture, chemicals, and corrosive gases [8,9]. Furthermore, its weldability, good formability, and availability make galvanized steel a technically and economically viable choice for use in demanding environments [10,11]. However, the presence of the zinc coating poses considerable challenges in resistance spot welding. Zinc exhibits relatively low melting (419 °C) and boiling (907 °C) temperatures. Zinc coating has low melting point, high conductivity and low resistance compared to the base low carbon steel. To carry out effective welding in the industry, current and welding times are set higher by 15–25 % as compared to uncoated steel, so that Zinc coating gets vaporized and sufficient heat can be generated . Increase in heat input reduces the electrode life and quality of the welded joint [12]. When galvanized sheets are welded, zinc near a weld molten pool evaporates. As a result, the corrosion resistance is deteriorated and repair coating treatment is required after welding [13]. These effects can degrade nugget quality, reduce joint strength, and impair the metallurgical soundness of the weld. To mitigate these problems, several approaches have been investigated over the past decade, including optimizing welding parameters [14]. Among these, the introduction of nanoscale reinforcements has received particular attention because of their ability to refine the microstructure, improve thermal distribution, and enhance the load-bearing capacity of the weld zone.

In recent studies, the addition of nanoparticles such as graphene [15], silicon carbide [16], and alumina [17] to the weld zone has led to improvements in hardness, wear resistance, and ultimate tensile strength. Specifically, SiC nanoparticles can improve load transfer and grain refinement through dispersion strengthening [18], while $Al_2O_3$ enhances hardness, oxidation resistance, and microstructural stability [19]. Graphene-based additives contribute to improved heat and electrical transfer, delaying crack initiation and enhancing the ductility and toughness of welded joints [20]. Among these, reduced graphene oxide (RGO) has gained significant attention due to its high strength-to-weight ratio, good thermal conductivity, and compatibility with metallic matrices, making it a promising reinforcement agent. Furthermore, RGO possesses residual oxygen functional groups that promote better interfacial bonding and homogeneous distribution in molten metal compared with pristine graphene, leading to more stable and uniform joint formation during the spot welding process. On the other hand, the recycling of industrial and metallic wastes such as machining chips holds considerable environmental and economic importance [21,22]. If not properly managed, these chips contribute to environmental pollution and loss of valuable mineral resources. By transforming these wastes into fine powders through mechanical milling and combining them with nanostructured reinforcements such as RGO, sustainable and cost-effective composite materials can be developed that simultaneously improve performance and reduce ecological impact. This study presents an innovative approach to improve the spot welding performance of galvanized steel sheets by applying a composite RGO/CK45 powder derived from recycled turning chips into the weld zone using a bio-based binder (tragacanth gum). This approach is designed to counteract the detrimental effects of zinc

penetration, enhance nugget integrity, and improve the overall mechanical response of the weld. The combination not only enhances the mechanical performance of the joint but also offers an environmentally friendly and cost-efficient route for industrial waste recycling. The novelty of this work lies in its integration of surface engineering, nanocomposite science, and welding technology with a recycling and sustainability perspective, contributing to the advancement of green and sustainable manufacturing processes in the metal industry.

## 2- Materials and Methods

In this study, aimed at enhancing the mechanical and biocompatible properties of spot welds in galvanized steel sheets, a composite powder made from recycled CK45 steel chips and reduced graphene oxide (RGO) was employed. The galvanized steel sheets used as the base material were industrial-grade with a thickness of 0.5 mm. The primary element in this alloy is iron (Fe), which is coated with a layer of zinc (Zn) to improve corrosion resistance. Other alloying elements such as carbon (C), silicon (Si), and manganese (Mn) are present in minor amounts and influence the microstructure and weldability of the galvanized steel. CK45 steel, known for its medium carbon content and high strength, was used as the source of metallic chips. This steel was machined under dry turning conditions (without lubricants) with cutting depths of 0.2, 0.3, and 0.4 mm to produce irregular but millable chips. The collected chips were thoroughly cleaned and dried, and X-ray diffraction (XRD) analysis was conducted to identify the chip condition with the closest phase match to the base metal. The selected chip sample was then subjected to mechanical milling to produce a fine powder.

Powder preparation was carried out using a planetary ball mill. A specific weight ratio of RGO and CK45 chips was placed in a steel milling chamber. To prevent contamination and unwanted oxidation, the milling process was conducted in a controlled atmosphere using zirconia balls. Milling was performed for 6 h at a speed of 300 rpm, resulting in a uniform mixture of steel particles and graphene nanosheets, with particle sizes reduced to below 100 microns. The presence of RGO in the composite enhanced the thermal conductivity and strength of the final powder, serving as both a structural and functional reinforcement. The RGO used in this study was synthesized using an improved Hummers method [23]. In this process, pure graphite powder was oxidized using a mixture of concentrated sulfuric acid, sodium nitrate, and potassium permanganate to obtain graphene oxide (GO). The GO was then reduced under controlled conditions using mild reducing agents such as ascorbic acid or hydrazine monohydrate to produce RGO. The reduction process decreased the oxygen-containing groups and partially restored the graphitic structure, significantly improving the mechanical and thermal properties. The resulting RGO powder was washed, filtered, and dried at 60°C before being combined with the machined steel chip powder. Subsequently, the CK45/RGO composite powder was mixed with a tragacanth gum solution to create a homogeneous mixture with suitable viscosity for localized application in the weld zone [24]. Tragacanth gum, a natural plant-derived resin, was selected for its biocompatibility, non-toxicity, and high structural stability. The gum was prepared at a defined concentration and uniformly mixed with the composite powder, which was then applied to the joining area between two galvanized sheets. Its role was to hold and localize the reinforcing particles within the weld area and prevent their migration or evaporation during the welding process.

In the final stage, prior to the resistance spot welding process, the galvanized steel sheets were mechanically polished using silicon carbide abrasive papers with grit sizes ranging from 400 to 2000, followed by thorough cleaning with ethanol and drying under ambie

conditions. The sheets were precisely aligned using a perforated alignment template, and the RGO/CK45 reinforcing mixture was injected into the designated weld zones .The welding operations were performed using an N-16KVA4546 resistance spot welding machine under controlled conditions. The key process parameters were kept constant throughout all experiments to ensure reproducibility and fair comparison between unreinforced, single-reinforced, and hybrid-reinforced joints. Specifically, the welding current was set to 9.5 kA, the electrode force to 3.5 kN, and the welding time to 12 cycles (0.24 s). These parameters were selected based on preliminary trials to achieve optimal nugget formation without expulsion.

After welding, the samples were prepared for mechanical and corrosion testing. All processing steps, from material preparation to welding, are schematically illustrated in Fig.1, and the material compositions and sample designations are summarized in Table 1. Post-weld analyses included tensile strength testing using a Universal Testing Machine (UTM) at a loading rate of 1.3 mm/min (ASTM A-370 standard) [25]. Phase identification was performed using X-ray diffraction (XRD) analysis with a GNR Explorer system operating at 40 kV and 30 mA. Morphological features were examined via scanning electron microscopy (SEM) using a TESCAN MIRA3 microscope with a resolution of 1.5 nm at an accelerating voltage of 15 kV. Electrochemical corrosion behavior was evaluated in the potential range of -250 to +250 mV, using a scan rate of 1 mV/s and an open circuit potential (OCP) stabilization time of 1200 sec.

**Table 1** – Material Properties Under Investigation

**Galvanized sheet**

| Element | Fe | C | Si | Mn | P | S | Ti | |
|---|---|---|---|---|---|---|---|---|
| Composition (%w) | 8.33 | 0.12 | 0.5 | 0.60 | 0.10 | 0.045 | 0.30 | |

**CK45**

| Element | Si | C | P | Mn | Ni | Mo | CR | S |
|---|---|---|---|---|---|---|---|---|
| Composition (%w) | 0.4 | 0.5 | 0.035 | 0.8 | 0.4 | 0.1 | 0.4 | 0.03 |

**RGO**

| Element | E | P | Elongation | Thermal conductivity | Electrical conductivity | |
|---|---|---|---|---|---|---|
| Composition | 1060 GPA | 1 g/cm$^2$ | 20% | 3000 W/MK | 15000 cm$^3$/v.s | |

**Sample name**

| Name | R1 | R2 | R3 | R4 | R5 | R6 | R7 | R8 |
|---|---|---|---|---|---|---|---|---|
| Composition | Galvanized | CK45 | Chip 0.2 mm | Chip 0.3 mm | Chip 0.4 mm | Weld without reinforcement | Weld+Chip 0.4 | Weld+Chip 0.4 + RGO |
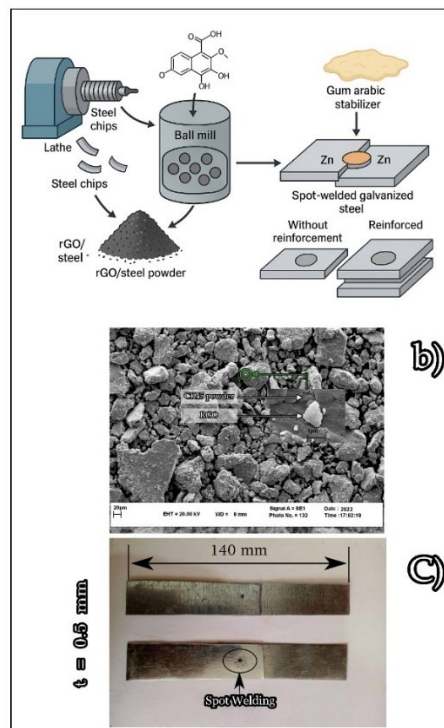


**Fig.1** Process Schematic : (a) *Schematic illustration of the process and experimental procedures,* (b) *SEM images of the reinforced powder mixture,* (c) *Welded specimens.*

## - Discussion and Conclusion

### 3-1 XRD Analysis

The presented X-ray diffraction (XRD) patterns illustrate significant structural variations among different samples, including the galvanized sheet, CK45 steel, machined chips at varying depths, and spot-welded specimens with and without reinforcement. The galvanized steel sheet shows three prominent diffraction peaks at 38.5°, 50°, and 75°, clearly indicating the primary crystalline phases associated with its stable surface zinc coating [26]. In contrast, the CK45 steel sample exhibits three main peaks at 45°, 65°, and 85°, reflecting its distinct alloy phase composition [27]. The shift in peak positions underscores the fundamental structural differences between the two materials, arising from their chemical compositions and processing routes. Machining chips obtained at cutting depths of 0.2, 0.3, and 0.4 mm exhibit not only the three characteristic peaks of the base CK45 steel but also smaller, scattered peaks. These secondary peaks suggest the presence of structural discontinuities and residual stresses induced by the intense mechanical action of the machining process [28]. As the cutting depth increases, the intensity and distribution of these minor peaks become more pronounced, indicating a greater degree of microstructural disruption and elevated internal stress [29]. The diffraction patterns of welded samples both unreinforced and those reinforced with chip powder or chip powder combined with RGO show distinct differences. The shift of main peaks toward lower angles and changes in intensity suggest the introduction of thermal stresses, compositional changes, and the possible formation of new phases in the weld zone [30]. The sample reinforced with RGO presents a notable and distinguishable peak at 26.5°, indicating the presence of reduced graphene oxide within the weld matrix [31]. The incorporation of RGO likely contributes to improvements in mechanical strength and corrosion resistance, playing a critical role in structurally and functionally enhancing the weld region.

A detailed examination of the XRD patterns confirms the direct influence of machining and welding processes on the crystalline structure and phase composition of the materials. These structural modifications such as internal stress generation, new phase formation, and incorporation of reinforcements like RGO correlate closely with the mechanical strength, corrosion behavior, and overall performance of the welded joints. Such findings are particularly valuable for high-performance applications in the oil, gas, petrochemical, and automotive industries, where the integrity of welded joints is of paramount importance. According to the XRD results, the chip labeled R5 was identified as the optimal reinforcing candidate due to its minimal phase deviation from the base metal and will be referenced as the selected reinforcement in the subsequent analyses.
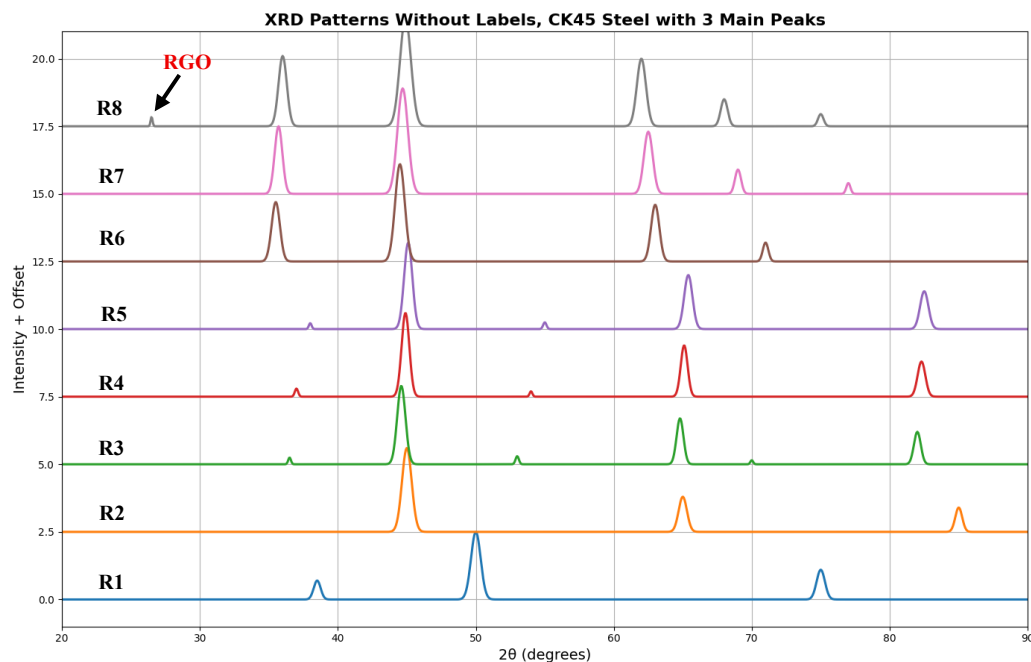


**Fig.2** XRD patterns of samples at different stages

### 3-2 Tensile Test

Tensile strength is a fundamental measure for assessing the quality of welded joints, as it directly reflects the efficiency of the applied welding parameters [32]. Analysis of the stress–strain curves from the tensile tests revealed notable differences among the three reinforcement conditions. The unreinforced sample exhibited the lowest mechanical performance, reaching a maximum load of 3100 N and yielding at a relatively low strain. This underperformance can be attributed to the absence of any strengthening agent in the weld zone, indicating a weak metallurgical bond within the joint. In contrast, the sample reinforced with recycled CK45 steel chip powder demonstrated a significant improvement, achieving a tensile load of 3500 N. The enhancement became even more pronounced in the sample reinforced with both chip powder and reduced graphene oxide (RGO), which withstood a maximum load of 4000 N. The steeper slope of its stress–strain curve illustrates the superior load-bearing capacity and better resistance to deformation. This marked increase in fracture load highlights the synergistic effect of combining metallic chips with RGO: the RGO acts as a reinforcement phase that improves stress distribution, controls microcrack propagation, and enhances

structural continuity in the weld zone. Importantly, these mechanical gains were achieved without compromising ductility, preserving the relative toughness of the joint a critical attribute for components exposed to impact and dynamic loading [33]. A distinctive aspect of this study is the strategic use of CK45 steel machining chips as a reinforcing material. Beyond lowering costs and reducing industrial waste, this approach facilitates targeted recycling. When paired with advanced nanomaterials like RGO, these chips markedly enhance the mechanical properties of the weld zone without the need for expensive additives. The stress–strain results clearly confirm the effectiveness of this strategy in reinforcing spot-welded joints, combining sustainability with superior mechanical performance.
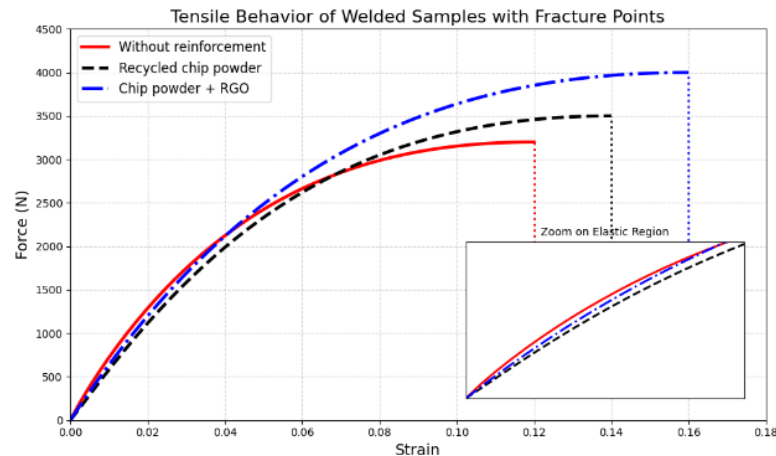


**Fig.3** Tensile test results

### 3-3 Combined Analysis of Elastic Modulus and Fracture Energy of Reinforced Spot-Welded Samples

The results obtained from mechanical testing reveal a significant enhancement in the mechanical properties of the reinforced spot-welded samples compared to the unreinforced ones. Specifically, the elastic modulus which reflects the material's resistance to elastic deformation increased from approximately 195 GPa for the unreinforced sample to 225 GPa in the sample reinforced with a combination of recycled machining chips and RGO. This increase in elastic modulus indicates a stiffening of the weld zone structure and improved load-bearing capability [34]. Furthermore, fracture energy, a crucial parameter for assessing toughness and resistance to crack propagation, also exhibited a notable improvement. According to the RILEM recommendation [35], the specific fracture energy ($G_f$) is defined as the total energy applied during a stable or quasi-stable fracture of a notched specimen, averaged over the projected fracture area. Let (P) denote the applied load, ($\delta$) the displacement at the loading point, (a) the initial crack (or notch) length, and (W - a) B the projected fracture area. The value of $G_f$ is then determined using the relation in which the symbol $G_f$ (a) is employed, since $G_f$ may depend on the ( a/W ) ratio or the specimen size. If necessary, the specimen's weight can also be considered in the calculation [35].

$$G_f\,(a) = \frac{1}{(w-a)B} \int P\,d\delta$$

The fracture energy increased from 5.8 kJ/m² in the unreinforced sample to 7.9 kJ/m² in the sample containing RGO. This upward trend indicates that the incorporation of recycled metallic particles and RGO nanoparticles improves stress distribution within the weld zone, reducing the likelihood of localized stress concentrations and enhancing resistance to fracture. Notably, the observed increase in the apparent elastic modulus in the reinforced samples can be attributed not to changes in the intrinsic bonding of the base metal, but to the effective load transfer between the metallic matrix and the dispersed reinforcing particles [36]. The RGO nanosheets and recycled metallic powder act as stiff inclusions that constrain local deformation and provide additional resistance against elastic strain, leading to a higher macroscopic elastic response of the composite weld zone. Consequently, the simultaneous improvement in both fracture energy and apparent elastic modulus demonstrates that reinforcing the weld zone with recycled powder and RGO enhances not only mechanical durability but also the structural stiffness under elastic loading. Such behavior is particularly advantageous in industrial applications, where welded joints must withstand high service loads while minimizing the risk of sudden failures due to crack initiation or propagation [37]. Furthermore, these findings highlight dual benefits: economic advantage through the reuse of machining chips, and functional enhancement through the improved mechanical performance of the welded joints.

As illustrated in Fig.4, brittle samples lacking sufficient weld nugget resistance showed little structural retention after fracture, whereas stronger samples maintained visible weld remnants, indicating more cohesive joint formation. Fractographic analysis revealed two dominant failure modes: interfacial failure and button pull-out failure [38]. Adhesive (interfacial) failure was observed in the absence of noticeable ductility, whereas plastic deformation predominantly led to fracture propagation along the weld seam. During tensile testing, low-strength specimens exhibited premature failure with negligible deformation, while high-strength counterparts, such as Sample R5, demonstrated pronounced bending and twisting behavior—further validating their superior weld integrity. Overall, the incorporation of recycled CK45 steel chips and RGO within the weld zone represents a technically feasible and environmentally sustainable strategy for enhancing the mechanical and structural performance of galvanized steel spot welds, particularly in high-demand automotive, construction, and structural engineering applications.
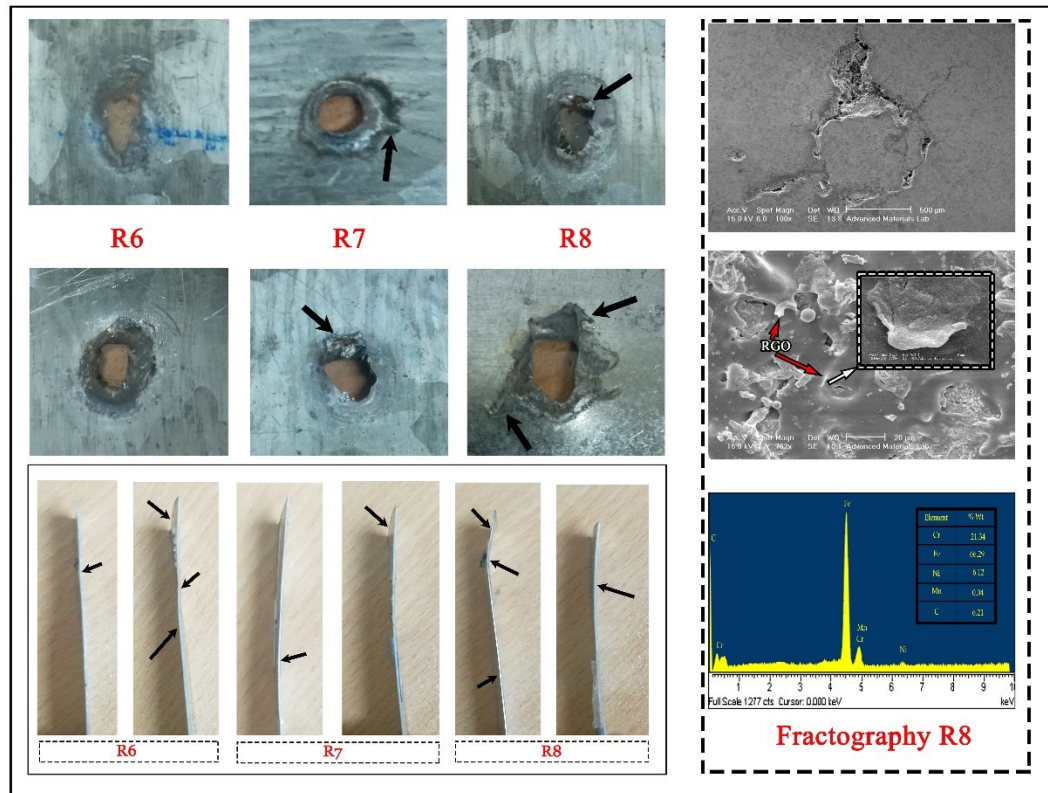
**Fig.4** (a) Types of spot weld fracture during the tensile test, (b) fractography of sample R8, (c) and (d) diagrams of elastic modulus and fracture energy for weld samples without reinforcement and with reinforcement. The increase in elastic modulus indicates enhanced elastic resistance in the weld zone, while the increase in fracture energy signifies improved toughness and greater resistance of the samples against crack propagation and mechanical failure.

## 3-4 Corrosion Test

In the potentiodynamic polarization test, the curves recorded in Fig.5a for the three welded samples indicate significant differences in corrosion resistance. The unreinforced sample exhibited a higher corrosion rate and a more negative corrosion potential ($E_{corr}$), indicating increased electrochemical activity and reduced stability in the corrosive environment [39]. Conversely, the sample reinforced with CK45 chip powder exhibited a more noble corrosion potential and a notably reduced corrosion current density. The most pronounced enhancement was achieved in the specimen incorporating a composite of CK45 chip powder and RGO, wherein the corrosion potential shifted toward less negative values and the corrosion current density ($I_{corr}$) reached its minimum among all tested samples. This observation confirms the improved passivation characteristics and the significantly reduced corrosion rate of the composite material.

Electrochemical impedance spectroscopy (EIS), analyzed via Nyquist plots, provided complementary insights into the corrosion mechanisms. Nyquist diagrams widely used to estimate the absolute electrical characteristics of materials such as grain boundary impedance and electrode interface properties were carefully examined [40]. In these plots, the diameter of the semicircular arcs directly correlates with charge transfer resistance and protective layer effectiveness [41]. Analysis of the Nyquist plots for samples R6, R7, and R8, shown in Fig.5b, revealed significant differences in electrochemical behavior attributable to surface structure, composition of resistive-capacitive layers, and ionic diffusion characteristics. Results indicated that the unreinforced sample exhibited the smallest arc diameter, reflecting low corrosion resistance [42]. Addition of chip powder increased the arc diameter, signifying enhanced electrochemical resistance [43].

The sample containing RGO displayed the largest arc diameter, indicative of the formation of a more stable passive layer and superior capacitive behavior at the surface interface. The R6 plot, characterized by a blue arc with an ideal semicircle angle of 180°, represents a stable and balanced electrochemical system where charge transfer resistance and capacitance operate harmoniously; this arc extends to about 200 $\Omega$ on the real axis, implying relatively low system resistance. In contrast, the R7 plot (black arc) shows an angle of 116° extending toward 300 $\Omega$ on the real axis, suggesting a less ideal response likely due to heterogeneities or distributed capacitive effects (constant phase element, CPE) commonly associated with defective or uneven surface coatings. Finally, the R8 plot (red arc), with a broad angle of 165° extending to approximately 700 $\Omega$, indicates a high surface resistance and extensive pseudo-capacitive behavior, which may be related to thicker layers, denser coatings, or multilayer structures. Comparing these plots confirms that R6 has the best electrochemical compatibility, R7 exhibits the most dispersed behavior, and R8 offers the highest electrolyte resistance among the tested systems.

The combined results of polarization and EIS tests demonstrate that the use of recycled CK45 machining chip powder as a reinforcing agent in the weld zone significantly enhances corrosion resistance. The presence of RGO, due to its layered structure, high specific surface area, and excellent conductivity, facilitates the formation of a uniform and stable protective film on the surface [44]. This effect is evident in both the reduction of corrosion current density in polarization tests and the increased impedance resistance observed in EIS measurements. Overall, the concurrent analysis of polarization and EIS tests not only validates the consistency of the results but also implies that employing recycled materials particularly in composite form with RGO presents a sustainable, cost-effective, and efficient strategy for improving the performance of galvanized steel spot welds in corrosive environments. These findings have practical implications for designing corrosion-resistant industrial joints, especially in automotive and steel structural applications.

Graphene-based materials, such as graphene oxide (GO) and reduced graphene oxide (rGO), possess remarkable resistance to the penetration of corrosive ions and function effectively as physical barriers. This capability originates from the dense stacking of their layers, which is attributed to the intrinsic $sp^2$ hybridized hexagonal structure of carbon atoms [45]. Furthermore, the large specific surface area, chemical inertness, and excellent stability of GO and rGO sheets serve as additional advantages, rendering them promising candidates for enhancing the corrosion resistance of protective coatings [46]. Moreover, owing to the lower content of oxygen-containing functional groups on both the edges and basal planes, rGO demonstrates superior water repellence and, consequently, higher hydrophobicity compared with GO [47].
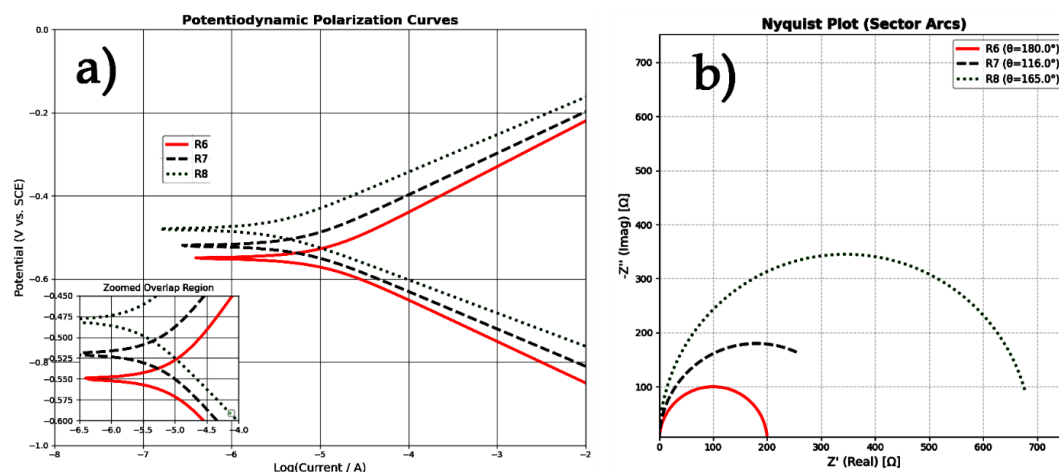


**Fig.5** Polarization curves illustrating corrosion potential ($E_{corr}$) and corrosion current density ($I_{corr}$) for the samples. b) Nyquist plots representing the electrochemical impedance behavior of the samples.

**Table 4** – Numerical results of the corrosion test

| Sample | $\beta_a$ (V/dec) | $\beta_c$ (V/dec) | $i_{corr}$ (A/cm²) | $E_{corr}$ (V vs SCE) | Rp (k$\Omega$·cm²) | Corrosion Rate (mm/year) |
|---|---|---|---|---|---|---|
| R6 | 0.11 | 0.10 | $1.0 \times 10^{-5}$ | -0.55 | 2.1 | 0.117 |
| R7 | 0.10 | 0.09 | $6.0 \times 10^{-6}$ | -0.52 | 4.3 | 0.070 |
| R8 | 0.09 | 0.08 | $3.0 \times 10^{-6}$ | -0.48 | 7.9 | 0.035 |

## 4- Conclusion

The findings of this study demonstrated that the localized application of a composite powder made from recycled CK45 steel machining chips and reduced graphene oxide (RGO) in the spot-weld zone of galvanized steel sheets acts as a multifunctional reinforcement, significantly enhancing both the mechanical and electrochemical properties of the joint.

1.     The tensile test results showed that the fracture load in the reinforced sample increased from 3200 N (unreinforced sample) to 4000 N, corresponding to a 25% improvement in weld zone strength.

2.     Galvanic corrosion testing and Nyquist analysis revealed a reduction in the corrosion rate from 0.117 to 0.035 mm/year, equivalent to a 70% decrease in corrosion rate. This improvement was attributed to the effective inhibitive performance of RGO, increased

electrochemical surface resistance, and decreased penetration of corrosive ions.

3.        The Nyquist plots indicated that the unreinforced sample (R6) exhibited an ideal capacitive behavior with a full 180° semicircle but lower surface resistance, whereas the sample containing recycled powder (R7) showed a less ideal but more resistant response with a 116° angle. Finally, sample R8, containing both RGO and recycled powder, displayed the widest angle of 165° and the highest real-axis resistance (~700 Ω), demonstrating superior electrochemical performance and corrosion inhibition.

Overall, this approach represents a green and effective technology for enhancing the durability and quality of spot welds in automotive, construction, and coated equipment industries.

**Ethics Approval**:
The scientific content of this article is the result of the authors' research and has not been published in any Iranian or international journal.

**Conflict of Interest**:
This article includes some results from the corresponding author's doctoral dissertation. There are no other conflicts of interest to declare.

# 5- References

[1] Adkine, A. S., & Biradar, S. K. (2025, February). A review of the effects of resistance spot welding on metallurgical and mechanical characteristics. Welding International, 39(2), 52–65. doi: 10.1080/09507116.2024.2419551

[2] Ibragimovich, J. A. (2025, July). Welding shops in automobile production UZ AUTO: Review, technologies, challenges and prospects. Modern American Journal of Engineering, Technology, and Innovation, 1(6), 309–314.

[3] Zhao, E., et al. (2025, September). Mechanical property curve of resistance spot welding for on-line monitoring of the welding quality. Journal of Manufacturing Processes, 150, 539–554. doi: 10.1016/j.jmapro.2025.06.061

[4] Chuenmee, N., et al. (2025, March). Machine learning for predicting resistance spot weld quality in automotive manufacturing. Results in Engineering, 25, 103570. doi: 10.1016/j.rineng.2024.103570

[5] Alaa, E., Farhan, F., & Haluk, M. (2024). Enhancing welding efficiency and reliability in unstructured environments: A computational analysis of spot-welded steel sheet connections. Journal of Electrical Systems, 20(6s), 2363–2370.

[6] Saini, A., & Rehalia, V. (2023). Assembly of portable spot-welding machine. International Journal for Research in Applied Science & Engineering Technology (IJRASET). doi: 10.22214/ijraset.2023.55640

[7] Zakharova, I. (2024). Welding processes in the restoration of industrial and energy facilities. Machinery & Energetics, 15(1). doi: 10.31548/machinery/1.2024.56

[8] Kapil, A., Vivek, V. A., & Daehn, G. (2025, June). Role of zinc coating on joint properties in impact spot welded Al 6111 aluminum alloy to galvanized high-strength low-alloy steel. Journal of Advanced Joining Processes, 11, 100276. doi: 10.1016/j.jajp.2024.100276

[9] Chaouki, A., et al. (2025, March). The effect of zinc bath formulation on the corrosion resistance of galvanized steel: A short review. ACS Omega, 10(10), 9809–9823. https://doi.org/10.1021/acsomega.4c08303

[10] Zhao, D., et al. (2022, December). Correlating electrode degradation with weldability of galvanized BH 220 steel during the electrode failure process of resistance spot welding. Crystals, 13(1), 39. doi: /10.3390/cryst13010039

[11] Almeida, I. L., et al. (2023, February). Numerical and experimental analysis of SAE 1010 thin steel sheets formability with and without galvanizing (GI-85). Journal of the Brazilian Society of Mechanical Sciences and Engineering, 45(2), 101. doi:10.1007/s40430-022-03977-y

[12] Thakur, A. G., & Nandedkar, V. M. (2014). Optimization of the resistance spot welding process of galvanized steel sheet using the Taguchi method. *Arabian Journal for Science and Engineering*, *39*(2), 1171-1176. doi: 10.1007/s13369-013-0634-x

[13] Kodama, S., Ishida, Y., Asai, K., Mizumoto, M., Namekata, T., & Nagasaki, H. (2010). Development of stainless steel welding wire for galvanized steel sheets. *Welding in the World*, *54*(1), R42-R48. doi: 10.1007/bf03263483

[14] Hamidinejad, S. M., Kolahan, F., & Kokabi, A. H. (2012). The modeling and process analysis of resistance spot welding on galvanized steel sheets used in car body manufacturing. *Materials & Design*, *34*, 759-767. doi: 10.1016/j.matdes.2011.06.064

[15] Becheikh, N., & Tashkandi, M. A. (2025). Continuous Drive Friction Welding of Graphene-Reinforced AA6061 Alloy: Innovative Approach to Enhance Mechanical and Thermal Properties. *Journal of Materials Engineering and Performance*, *34*(8), 6951-6962. doi: 10.1007/s11665-024-09650-w

[16] Ponnusamy, V., Muthaiyan, R., Subramanian, S., & Govindasamy, R. (2025). Silicon carbide nanoparticle-enabled strengthening of aluminum and copper resistance spot welds. *Materials Science*, *31*(2), 171-176. doi: 10.5755/j02.ms.38335

[17] Habba, M. I. A., Ahmed, M. M. Z., Fouad, R. A., & Barakat, W. S. (2025). Friction stir welding of AA6082-T6 assisted with a novel encapsulated alumina interlayer: surface morphology, tribology, and topographic analysis. *The International Journal of Advanced Manufacturing Technology*, *139*(5), 2823-2845. doi: 10.1007/s00170-025-16063-z

[18] Foong, P. Y., Voon, C. H., Lim, B. Y., Teh, P. L., Yeoh, C. K., Parmin, N. A., ... & Perumal, V. (2025). Microwave Welding of Polypropylene Using SiC Nanowires as Susceptors: Effect of Silane Modification on Joint Performance. Journal of Materials Engineering and Performance, 1-13. doi:10.1007/s11665-025-11477-y

[19] Sabry, I., & El-Deeb, M. S. (2025). Enhanced structural integrity and tribological performance of Al6061–Al6082 alloys reinforced with TiB2 and Al2O3 via friction stir welding. The International Journal of Advanced Manufacturing Technology, 1-18. doi: 10.1007/s00170-025-15706-5

[20] Becheikh, N., & Tashkandi, M. A. (2025). Continuous Drive Friction Welding of Graphene-Reinforced AA6061 Alloy: Innovative Approach to Enhance Mechanical and Thermal Properties. Journal of Materials Engineering and Performance, 34(8), 6951-6962. doi:10.1007/s11665-024-09650-w

[21] Chen, X., Saada, M. B., Lavisse, B., & Ammar, A. (2025). Recent advances in the remelting process for recycling aluminium alloy chips: a critical review. *International Journal of Material Forming*, 18(2), 42. doi: 10.1007/s12289-025-01904-9

[22] Alavizadeh, S. A. R., Shahbaz, M., Kavanlouei, M., & Kim, S. S. (2025). The effect of mechanical milling for enhanced recycling Ti6Al4V powder from machining chips. *Scientific Reports*, 15(1), 444. doi: 10.1038/s41598-024-84913-z

[23] Attari, K., et al. (2025, June). Applications of graphene, graphene oxide, and reduced graphene oxide on cotton fabric. Cellulose, 1–45. doi: 10.1007/s10570-025-06600-0

[24] Khosravi, M., et al. (2020). Effect of graphene oxide and reduced graphene oxide nanosheets on the microstructure and mechanical properties of mild steel jointing by flux-cored arc welding. International Journal on Minerals, Metallurgy, and Materials, 27, 505–514. doi: 10.1007/s12613-020-1966-7

[25] Balakrishnan, K. S., Samal, M. K., Parashar, J., Tiwari, G. P., & Anatharaman, S. (2014). Suitability of miniature tensile specimens for estimating the mechanical property data of pressure tubes: an assessment. *Transactions of the Indian Institute of Metals*, 67(1), 47-55. doi:10.1007/s12666-013-0316-0

[26] Zorlu, R., et al. (2024, August). Development of a novel hydrothermal process for surface modification of galvanized steel, characterization, and photocatalytic application. Surfaces and Interfaces, 51, 104780. doi:10.1016/j.surfin.2024.104780

[27] Wang, J., et al. (2024, October). A comprehensive review of metal laser hardening: Mechanism, process, and applications. The International Journal of Advanced Manufacturing Technology, 134(11), 5087–5115. doi: 10.1007/s00170-024-14463-1

[28] Bao, F., et al. (2024). Interface-reinforced ceramic coatings via Type-B2 discharge in micro-arc oxidation: A dual-stage strategy for enhancing wear-corrosion resistance of bearing steel. SSRN Electronic Journal. doi:10.2139/ssrn.5334771

[29] Li, L., et al. (2025, May). Enhancing impact toughness in 904L stainless steel welded joints using ultrasound-assisted laser welding without sacrificing strength and ductility. Journal of Materials Research and Technology, 36, 4476–4489. doi: 10.1016/j.jmrt.2025.04.112

[30] Chege, D. W. (2024). Effect of thermal insulation and welding parameters on residual stresses of welded joints (Ph.D. dissertation). College of Engineering and Technology (COETEC), JKUAT.

[31] Cruz, B. D., et al. (2024, August). Polyethylene of raised temperature resistance (PE-RT) nanocomposites reinforced with graphene oxide for application in flexible pipelines. Materials Research, 27, e20240124. doi: 10.1590/1980-5373-mr-2024-0124

[32] Liu, J., et al. (2024, April). Prediction and optimization method for welding quality of components in ship construction. Scientific Reports, 14(1), 9353. doi:10.1038/s41598-024-59490-w

[33] Zhang, Q., et al. (2025, March). Advances and challenges in interference-fit technology for enhancing the mechanical performance of joints. Journal of Materials Engineering and Performance, 34(5), 3585–3607. doi: 10.1007/s11665-024-10418-5

[34] Aghajani, H., Bahrami, M., & Pouranvari, M. (2024, May). Enhancing load-bearing capacity of martensitic stainless steel resistance spot welds: Microstructural vs. geometrical approaches. Materials Science and Engineering: A, 901, 146508. doi: 10.1016/j.msea.2024.146508

[35] Hu, X. Z., & Wittmann, F. H. (1992). Fracture energy and fracture process zone. Materials and Structures, 25(6), 319-326. https://doi.org/10.1007/bf02472590

[36] Sedehi, S. M. R., Khosravi, M., & Yaghoubinezhad, Y. (2021). Mechanical properties and microstructures of reduced graphene oxide reinforced titanium matrix composites produced by spark plasma sintering and simple shear extrusion. Ceramics International, 47(23), 33180-33190. doi:10.1016/j.ceramint.2021.08.219

[37] Karmakar, S. (2024, June). Impedance spectroscopy for electroceramics and electrochemical systems. arXiv preprint arXiv:2406.15467. doi: 10.37256/aecm.6120255567

[38] Zhao, Y., et al. (2024, December). Failure mechanisms of hybrid metal–composite joints with different protrusion densities under a tensile load. Mechanics of Advanced Materials and Structures, 31(24), 6150–6165. doi:10.1080/15376494.2023.2226129

[39] Kollabathini, S. S., Dora, S. P., & Chintada, S. (2025, January). Corrosion behaviour of advanced composites containing surface modified SiC as reinforcement. Journal of Alloys and Compounds, 1010, 177423. doi: 10.1016/j.jallcom.2024.177423

[40] Volchkov, S. O., et al. (2021, October). Magnetoimpedance of CoFeCrSiB ribbon-based sensitive element with FeNi covering: Experiment and modeling. Sensors, 21(20), 6728. doi: 10.3390/s21206728

[41] Ma, Z., et al. (2025, March). A novel Ta/TaN/TaAlN nanocrystalline coating on metal bipolar plates with excellent corrosion resistance. Journal of Power Sources, 632, 236307. doi: 10.1016/j.jpowsour.2025.236307

[42] Yang, G., et al. (2024, April). Effect of chloride salt types on corrosion resistance of reinforcing steel in cement mortar mixed with DNA primer inhibitor. Cement and Concrete Composites, 148, 105454. doi: 10.1016/j.cemconcomp.2024.105454

[43] Thangamuthu, M., et al. (2024). From scrap metal to highly efficient electrodes: Harnessing the nanotextured surface of swarf for effective utilization of Pt and Co for hydrogen production. Journal of Materials Chemistry A, 12(25), 15137–15144. doi: 10.1039/d4ta00711e

[44] Shingte, S. R., et al. (2025, January). The power trio: $CoS–CoFe_2O_4–rGO$ ternary composite to enhance energy density of all-solid-state asymmetric supercapacitors. Journal of Energy Storage, 106, 114842. doi: 10.1016/j.est.2024.114842

[45] R.F. Albers, R.A. Bini, J.B. Souza Jr., D.T. Machado, L.C. Varanda, A general one-pot synthetic strategy to reduced graphene oxide (rGO) and rGO-nanoparticle hybrid materials, Carbon 143 (2018) 73–84. doi: 10.1016/j.carbon.2018.10.087

[46] V. Mišković-Stanković, I. Jevremović, I. Jung, K. Rhee, Electrochemical study of corrosion behavior of graphene coatings on copper and aluminum in a chloride solution, Carbon 75 (2014) 335–344. doi: 10.1016/j.carbon.2014.04.012

[47] J. Quezada-Rentería, L. Cházaro-Ruiz, J. Rangel-Mendez, Synthesis of reduced graphene oxide (rGO) films onto carbon steel by cathodic electrophoretic deposi- tion: anticorrosive coating, Carbon 122 (2017) 266–275. doi: 10.1016/j.carbon.2017.06.074